DOI: 10.13009/EUCASS2023-612
Aerospace Europe Conference 2023 – 10TH EUCASS – 9TH CEAS

Field reconstruction of the spacecraft from limited sensors based on graph neural networks

Qiao Li[1], *Xingchen Li*[2,3,†], *and Wen Yao*[2], 3,
[1]*College of Aerospace Science and Engineering, National University of Defense Technology, 410072, Changsha, China*
[2]*National Innovation Institute of Defense Technology, Academy of Military Science, 100071, Beijing, China*
[3]*Intelligent Game and Deision Laboratory, 100071, Beijing, China*
10213470@qq.com · lixingchen14@nudt.edu.cn · wendy0728@126.com
[†]Corresponding author

Abstract

With the development of space technology, how to realize the real-time and high-accuracy prediction of the spacecraft? Physical field plays an important role in intelligent control and status detection. Traditionally, this is achieved by some sensors at the key location. However, the sensors provide limited information about the spacecraft. Thus, reconstructing the physical field can greatly improve the status detection of the spacecraft. Moreover, considering the subsystems within a spacecraft?s close relationships, we have proposed the field reconstruction of the spacecraft based on graph neural networks. Firstly, we model the subsystems of a spacecraft into a mathematical graph and embed the relationships between the subsystems and the monitoring sensors by the edges of graph. Then we construct a graph neural network to extract the hidden features of the limited sensors through an encoder and obtain the whole physical field of the spacecraft via a decoder. As one of the deep learning models, the graph neural network can provide a real-time prediction of the field, and the embedding of the relationships within the spacecraft could help improve the precision of the final prediction. By this graph neural networks, we have realized the real-time and high-precision reconstruction of the whole field, which can help the intelligent control and status detection of a spacecraft.

1. Introduction

Monitoring and perceiving status information of spacecraft is the foundation for its analysis and control. The traditional route is to deploy sensors in essential positions to measure spacecraft status. However, the sensor will occupy the interior space of spacecraft to hinder equipment miniaturization. Meanwhile, the information measured by sensors is usually limited, so it is difficult to monitor the full status to meet the needs of fine management of spacecraft. Therefore, it is valuable to recover full status from limited measurements[1,2] to reduce the placed sensors or increase the perceived information. In particular, digital twinning technology[3] has been applied to various natural systems, including the spacecraft, and one of critical challenges is to reconstruct full-state of physical systems combined with the sensor data. Motivated by the above-mentioned problems, this work focuses on the physical field reconstruction of spacecraft with limited sensors.

One challenge of field reconstruction problem is that it is often ill-posed because of the limited exact measurements, and solving the inverse problem by numerical method may not yield satisfactory results. Recent studies have made progress in learning how to recover unknown information from offline data by data-driven paradigm, especially for that deep learning-based reconstruction methods have shown remarkable performance in many scenarios. For deep learning-based reconstruction methods, deep neural networks (DNNs) stacked with deep layers for powerful approximation capacity are employed to learn the mapping from sparse measurements to global physical field.

In existing research, there are two routes to leverage DNNs for field reconstruction: model reduction-based methods[4] and end-to-end methods. Traditional model reduction-based methods are independent of DNNs. It is a learning paradigm to explicitly decompose the field reconstruction task into two steps: reduced order model (ROM) establishment and low-dimensional coefficients estimation. ROMs[5–7] is usually used to simplify the complex and high-dimensional full-order physical model by low-dimensional representations that can approximate the original model well. The major advantage of ROMs is saving computational resources and avoiding producing the costly and time-consuming high-fidelity physical field. As the representative ROMs, proper orthogonal decomposition (POD)[8,9] and

DOI: 10.13009/EUCASS2023-612

dynamic mode decomposition (DMD)[10] generate reduced basis, which can be linearly combined[11] to estimate the global field. Then, the key step for field reconstruction is to obtain the combination coefficient by solving an optimization problem[12–14] estimating by building regression models. The capacity of traditional linear ROMs is limited that some researchers explore to build parameterized ROMs[15] by DNNs, aiming to improve dimensionality reduction performance by the non-linear approximation ability effectively. The DNN architectures for building ROMs include autoencoder,[16,17] generative model,[18,19] etc. Besides, the DNNs can be employed to improve low-dimensional coefficient estimation accuracy by establishing deep regression models.[20] Some studies[7,21] have shown that model reduction-based methods with DNN can outperform traditional ROMs regarding representation ability and reconstruction performance. However, model reduction-based methods have some drawbacks to affect the reconstruction performance. Firstly, it introduces errors in both ROMs building and coefficients estimation stages, which may increase the reconstruction errors. Secondly, the stage for dimensionality reduction will bring the loss of information and suffer from generalization issues to hurt method performance.

This paper aims to propose a novel end-to-end field reconstruction method from limited measurements using deep neural networks. Unlike ROM-based methods to decompose field reconstruction into two stages, end-to-end methods exploit various network architectures to directly learn the mapping from sparse observations to the global physical field. In existing methods, fully-connected neural networks (FCNN) and convolutional neural networks (CNN) are the two main architectures for end-to-end reconstruction learning. Compared with POD-based methods, some studies[22] have shown that FCNN can achieve better results in some flow field reconstruction problems. However, FCNN usually suffers from low efficiency problem especially when making large-scale and structured predictions.

In contrast, CNNs have better computational efficiency benefiting from parameter sharing, and have become the state-of-the-art methods in various tasks.[23,24] Therefore, deep CNNs have been widely used in various physical field reconstruction problems. Since CNNs are originally developed for computer vision to handle image data, the input data should be transformed into image-like data. One way for the unstructured and sparse measurements from sensors is to adopt fully-connected layers to project measurements into high-dimensional representation,[25] and then reshape it to feature maps as the inputs of CNN block. Another way is to adopt a well-designed form to represent measurements. For example, Gong et al.[26] and Peng et al.[27] proposed to use mask representations that the sensor positions are padded with observed values and others are zeros, and an image-to-image architecture using CNN is developed for temperature field reconstruction. Avoiding pad zeros in the unobserved positions,[28] designed more robust representations named Voronoi to divide the computational domain into several regions, in which a specific observation is allocated to pad the region with observed value rather than zeros.

In conclusion, CNN is difficult to handle unstructured inputs and outputs due to its structure. However, the data generated by numerical simulation or collected from practical experiments is usually unstructured. For example, the unstructured meshes and local grid refinement are widely performed in various numerical simulations of spacecraft to obtain accurate solutions. In practice, sensors are usually unevenly arranged to monitor the status in important positions. Therefore, existing network architecture has limitations to some extent to meet practical needs. Graph neural networks (GNNs) are deep learning models that can learn from graph-structured data, such as social networks, molecular structures, knowledge graphs, etc. Since graphs can conveniently represent various complex data forms, it is promising to model the unstructured measurements and physical field as graphs and employ GNNs to achieve end-to-end field reconstruction. Graph convolutional networks (GCNs) generalize the concept of convolution from regular data domains (such as images) to irregular data domains (such as graphs). The key idea of GCNs is to learn a function that fuses the features of a node and its neighbors to produce a new representation of the node. GraphSAGE is developed based on GCNs to improve efficiency in processing large-scale graphs. The core of GraphSAGE is to sample neighbor nodes for each node and aggregate information from neighbors by aggregation function. Graph neural networks have achieved great success in various learning tasks on graphs.

There are few researches on graph neural networks for physical field reconstruction and predictions. Han et al.[29] developed a subequivariant graph neural network to model the physical dynamic of multiple interacting objects that can accurately capture the physical dynamic and exhibit strong generalization. Chen et al.[30] proposed a GCNs structure as a surrogate model to learn laminar flow prediction around random two-dimensional shapes. Similar to the field reconstruction task at hand, Pata et al.[31] leveraged GNNs to present an end-to-end trainable, machine-learned particle-flow algorithm. For the field prediction of spacecraft, Bonnet et al.[32] developed a dataset to predict the incompressible flow over airfoils and evaluate the performance of GNNs in these deep learning baselines.

In conclusion, graph neural network for physical field prediction and reconstruction is in the preliminary stage. Inspired by the potential performance of GNNs for complex data structures and irregular regions, this paper aims to introduce the graph neural network to handle field reconstruction task of spacecraft from limited measurements. Firstly, the measurements and physical field are represented with graph, and the objective is to learn to recover the unknown information on graph from historical data. The graph is more flexible than image representations for CNN and can better preserve correlation in spatial than vector representations for FCNN. Secondly, graph convolutional networks

DOI: 10.13009/EUCASS2023-612

(GCNs) and GraphSAGE, two classical GNN arcarchitecture? are employed to update the state embedding vector in each node by the information propagation and aggregation on the graph. The multi-layers architecture enables GNNs to learn complex mapping relationships. The contributions of this work are as follows:

- A connected graph is used to represent physical field and exact measurements on it, and physical field reconstruction for spacecraft is modeled as a learning task on graphs, which has better applicability for irregular regions and unstructured data.
- A field reconstruction method based on graph neural networks is developed to extract features on graph to capture the correlation between unknown nodes and exact measurements.
- Experiments on thermal and flow field reconstruction are conducted to demonstrate that the GNN-based reconstruction method can accurately recover unknown information from limited observations.

The remainder of the article is organized as follows. The field reconstruction problem of spacecraft from limited sensors is described in Section 2. Section 3 introduces the proposed GCNs-based reconstruction method, consisting of a comprehensive framework, graph representation, and graph convolution neural networks. Section 4 presents and discusses the results of thermal and fluid numerical experiments. Section 5 concludes the whole article.

2. Problem Description

Assume that the physical field of spacecraft is determined by the inherent physical law that depends on the system parameters $\boldsymbol{\lambda} \in \mathbb{R}^{n_\lambda}$ and time $t \in \mathbb{R}$. Without loss of generality, the nonlinear function $f(\cdot)$ is introduced to describe the mapping relationship between physical field and system parameters as follows:

$$\boldsymbol{s} = f(t; \boldsymbol{\lambda}). \tag{1}$$

where $\boldsymbol{s} \in \mathbb{R}^{N_s}$ is the discretization of two-dimensional or three-dimensional field. The sparse observations $\boldsymbol{o} \in \mathbb{R}^n$ are measured at n locations over the global field, where $n \ll n_s$. The global field $\boldsymbol{s}$ is the target of reconstruction from the sparse observations $\boldsymbol{o}$. This is an challenging inverse problem that requires inferring high-dimensional unknown information from low-dimensional observations.

Data-driven paradigm in this work to learn the reconstruction mapping from historical data. The data-driven method consists of offline and online stages. In the offline stage, the snapshots matrix $\boldsymbol{S} = (\boldsymbol{s}_i) \in \mathbb{R}^{N \times N_s}$ is constructed by collecting and storing the global fields. Using the offline snapshots, data-driven methods aim to learn the mapping $g(\cdot)$ with parameters θ from the observations to the global field by neural networks or other regression models, which can be written as

$$\boldsymbol{s}' = g(\boldsymbol{o}; \theta). \tag{2}$$

In this work, the physical field is represented by a connected graph, and the reconstruction mapping is approximated on graph. Denoted a simple and connected undirected graph $G = (V, E)$ with n nodes and m edges, A is the adjacency matrix. Each node represents one target value in the physical field, and nodes are connected according to the distance in computational domain. First, the sparse measurements $\boldsymbol{o}$ are projected to the inital embedding $e_i \in \mathbb{R}^{n_0}$ of each node, and the initial feature matrix is $H^{(0)} \in \mathbb{R}^{n \times n_0}$, which represents the status of graph $G(0)$ in the first stage. The process can be expressed as

$$H^{(0)} = e(\boldsymbol{o}) \tag{3}$$

Then, the graph neural network g is employed to update the feature in each node, and produce the final feature matrix $H^{(k)}$. Finally, the value in each node is obtained by a decoder d. The mapping will be learned in this work can be described as:

$$\boldsymbol{s}' = d_\theta \circ g_\theta \circ e_\theta(\boldsymbol{o}) \tag{4}$$

Utilizing historical data for learning, the parameterized network is expected to generalize to unknown measurements and provide the field reconstruction results in real-time.

3. Methods

In this section, the field reconstruction architecture based on graph neural network is first introduced. Moreover, the essential components of architecture, consisting of graph representation for observations, graph convolutional network, and GraphSAGE network, are described in detail.

DOI: 10.13009/EUCASS2023-612

3.1 Overall Architecture

The architecture of the proposed reconstruction method is shown in Fig. 1. Taking the thermal field reconstruction for heat source system as example, the physical simulation or practice experiments are firstly conducted to generate snapshots for model training, in which sparse measurements at the locations of sensors are used as inputs and global field data as labels. To leverage the graph neural network, the whole domain is seen as a connected graph, and each status value in physical field is the node of graph. The Euclidean distance in the computational domain determines the edge between different nodes. This work establishes the edges between each node and its *kth* nearest nodes. After that, the graph is constructed, and the measurements from limited sensors are projected as the graph embedding in each node. Then, the GCN and GraphSAGE networks are employed to extract features on the graph and produce the reconstruction results. Once the network has been trained, when the measurements from sensors are collected in practice, the trained model can fast produce the reconstructed field to support analysis and control of the management system.

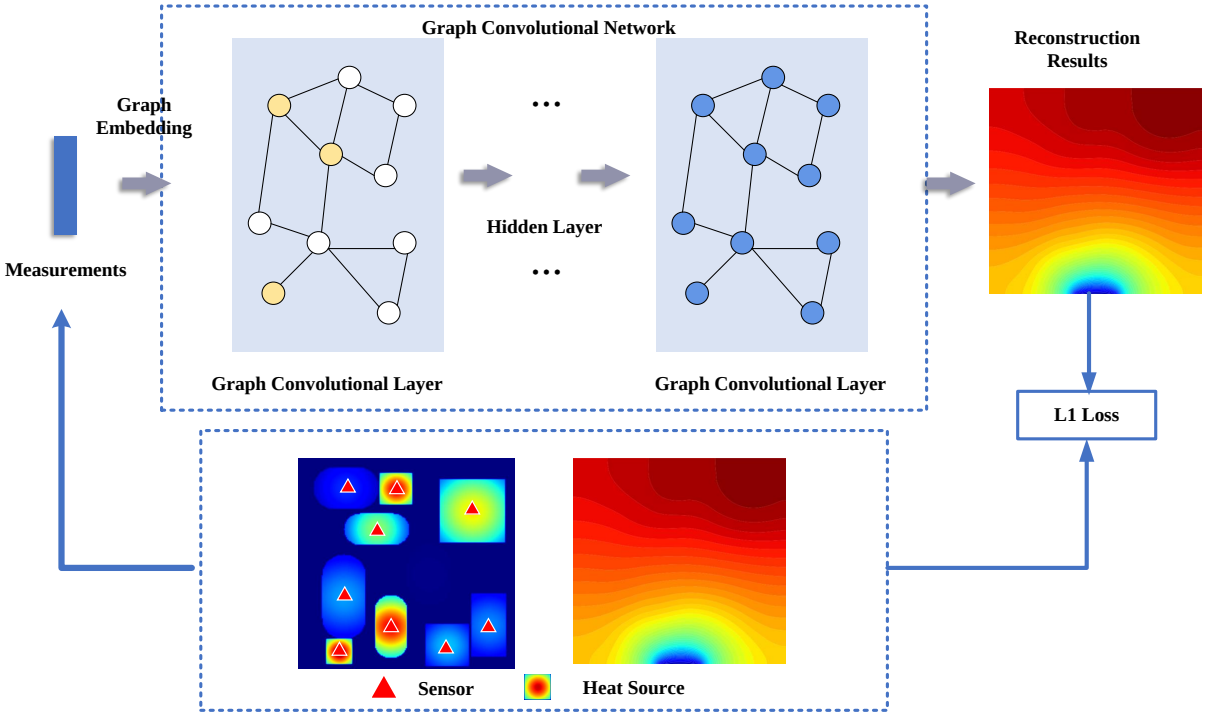

Figure 1: Schematic of the global field reconstruction method via graph convolutional network.

3.2 Graph Representation

Graph representation consists of graph construction and graph embedding generation. Assume that position of each node in the field is known, and graph edges are generated according to the Euclidean distance between different nodes. Specifically, each node is connected with its k nearest to establish an undirected graph. Graph embedding is the initial status of each node. For a graph $G = (V, E)$ with n nodes, fully-connected layers are employed to project the sparse measurements $\boldsymbol{o}$ into high-dimensional vector $\boldsymbol{c} \in \mathbb{R}^n$. In each node i, the produced value is concatenated with the position vector $\boldsymbol{p}_i \in \mathbb{R}^2$ as the graph embedding $\boldsymbol{e}_i^{(0)} \in \mathbb{R}^3$. At the first stage, the feature matrix of graph is n matrix $\boldsymbol{H}^{(0)} \in \mathbb{R}^{n\times 3}$, which are prepared as the inputs of graph neural network for an update.

Graph representation has better flexibility compared with others. Fig. 2 shows existing representation forms for filed reconstruction problems, consisting of vector, image, and graph representations. Sparse measurements and field data are expanded as vectors, suitable for various applications. However, the spatial information is not preserved with expansion, and an efficiency issue exists when employing FCNN to handle high-dimensional vectors. Image is a good choice for structured data because of spatial information preservation and advanced performance of various image-to-image network architectures. Graph is a clear and ideal representation to model the relationship among

DOI: 10.13009/EUCASS2023-612

different points flexibly. Graph neural networks are good at learning on graphs and progress greatly on social networks, molecular structures, and knowledge graphs. To investigate the performance of GNN in physical field prediction and reconstruction task, the next section introduces GCN or GraphSAGE as a surrogate model to reconstruct physical field from limited measurements.

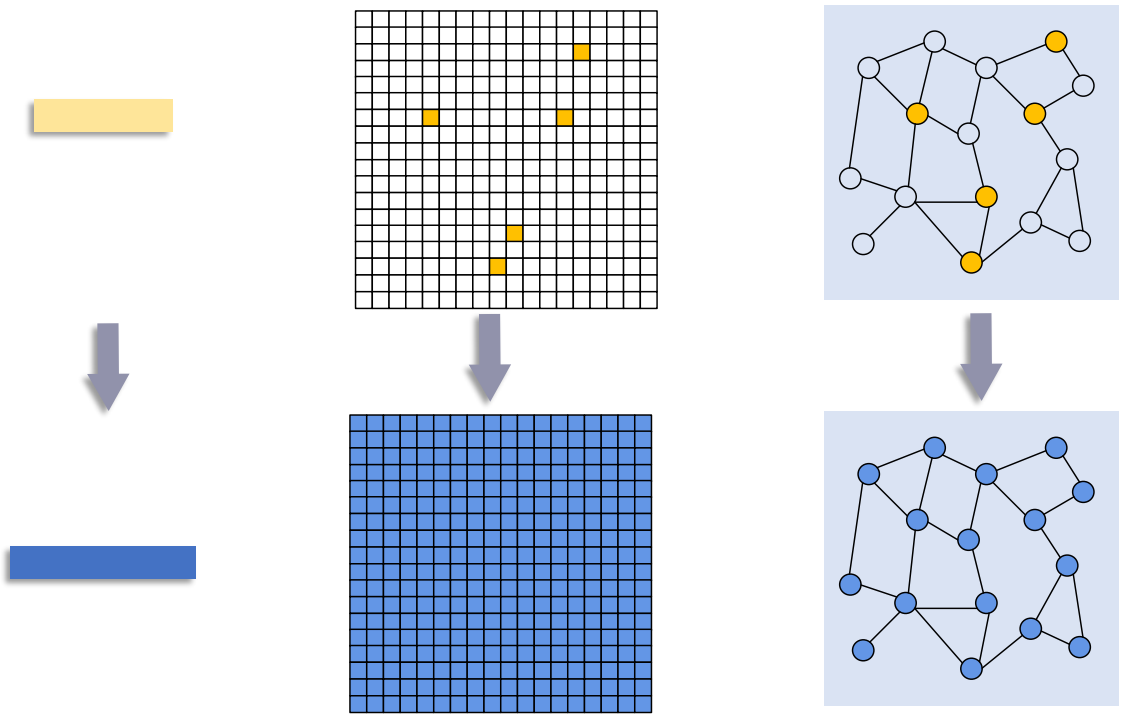

(a)vector (b)image (c)graph

Figure 2: Schematic of vector, image, and graph representations.

3.3 Graph Convolution Network

GNNs consist of two main components: a message-passing mechanism that aggregates information from neighboring nodes in the graph and a readout function that produces a global representation of the graph or a local representation of each node. Denoted a graph $G = (V, E)$ contains n nodes, and the feature of node v_i in lth stage is $e_{v_i}^{(l)} \in \mathbb{R}^{d_l}$. Therefore, the feature of all nodes lth stage can be represented by feature matrix $H^{(l)} \in \mathbb{R}^{n \times d_l}$. Based on the principle of feature aggregation in each graph convolution layer, feature matrix $H^{(l+1)}$ in the next stage by one convolution operation can be expressed as:

$$H^{(l+1)} = \sigma\left(\tilde{\mathrm{D}}^{-\frac{1}{2}}\tilde{\mathrm{A}}\tilde{\mathrm{D}}^{-\frac{1}{2}}H^{(l)}W^{(l)}\right) \tag{5}$$

$$\tilde{A} = A + I \tag{6}$$

where A and I are adjacent matrix and unit matrix. $\sigma(\cdot)$ is non-linear activation function, and the $W^{(1)}$ is learnable paramters in current stage l. $\tilde{D}$ is the degree matrx of adjacent matrix $\tilde{A}$, which is calculated by:

$$\tilde{D} = \sum \tilde{A}_i^j \tag{7}$$

A graph convolutional layer aggregates the features of neighbors of each node by a weighted sum and transforms them into new features by multiplying with a learnable matrix. By computing the features of all nodes in a matrix form and applying convolution operations through layer-wise propagation, the node features are updated in the end.

DOI: 10.13009/EUCASS2023-612

3.4 GraphSAGE

GraphSAGE is a spatial-based graph neural network model that can leverage the attribute information and structural information of nodes to generate node embeddings. The main idea of GraphSAGE is to update the node information based on its own and neighbor information. Two main components of GraphSAGE are sampling and aggregation, which are the source of the method name. The diagram of GraphSAGE can be divided into three stages:

Neighbor nodes sampling. For computational efficiency, partial neighbor nodes are sampled to be aggregated for each node. Let the sampling number be k. If the number of neighbor nodes is less than k, a sampling method with replacement is used until k nodes are sampled. If the number of neighbor nodes is greater than k, a sampling method without replacement is used. Of course, if computational efficiency is not considered, all the neighbor nodes can be used for information aggregation.

Information aggregation. The information contained in the neighbor nodes is aggregated according to the aggregation function. Since the neighbor nodes in the graph are naturally unordered, the aggregation function is hoped to be symmetric and has high expressive ability. The common aggregation aggregators include mean aggregator, pooling aggregator, and LSTM aggregator. In this paper, the mean aggregator is adopted as follows:

$$H_v^{(l)} \leftarrow \sigma\left(W \cdot \text{mean}(\{H_v^{(l-1)}\} \cup \{H_u^{(i-1)}, \forall u \in N(v)\})\right) \tag{8}$$

where $N(v)$ is the neighbor nodes set of nodes v. The neighbor nodes sampling stage determines the set $N(v)$.

Parameters optimization. The aggregated features are first used to make predictions, and then the loss function between the prediction results and the labels is calculated. Use the backpropagation algorithm to optimize the neural network parameters.

4. Results and discussion

The experiments are conducted on three problems, including 2D steady-state thermal field reconstruction for heat source system, 2D compressible flow field over airfoil, and a practical case from an on-orbit satellite. GCN and GraphSAGE networks are implemented in three problems. The performance of different methods is evaluated by the mean absolute error MAE $= \left\|\mathbf{u} - \mathbf{u}_p\right\| / |\mathbf{u}|$. MAE metric measures the gap between predicted field $\mathbf{u}_p$ and labels $\mathbf{u}$, where $|\mathbf{u}|$ is the total number of points for reconstruction.

4.1 Steady-state Thermal Field Reconstrcution for Heat Soure System

The first case is to reconstruct steady-state temperature field for heat source system,[33,34] such as chips and satellite.[35] The reconstructed thermal field with limited sensors can assist in the thermal monitoring of heat source systems. The heat source system is shown in Figure 3 that some Gaussian heat sources are placed on a square computational domain $\Omega = [0, 0.1] \times [0, 0.1]$. The middle bottom boundary is a thermostatic heat sink of 0.01 length to dissipate generated, and the others are adiabatic. The steady-state thermal field of heat source system can be described as follows:

$$\begin{aligned} &\tfrac{\partial}{\partial x_i}\left(\lambda \tfrac{\partial T}{\partial x_i}\right) + \tfrac{\partial}{\partial x_j}\left(\lambda \tfrac{\partial T}{\partial x_j}\right) + \phi(x_i, x_j) = 0 \quad && (x_i, x_j) \in \Omega, \\ &T(x_i, x_j) = T_D && (x_i, x_j) \in \partial\Omega_D, \\ &\lambda \tfrac{\partial T(x_i, x_j)}{\partial n} = 0 && (x_i, x_j) \in \partial\Omega_N, \end{aligned} \tag{9}$$

where Ω_D is the boundary condition of heat sink, and Ω_N are the adiabatic boundaries. The conductivity coefficient is λ, which is determined by $\lambda = 1 + 0.05 \times (T - 298)$.

The experiments in this section aim to recover thermal field of heat source system with different heat intensities $\phi(x_i, x_j)$ and boundary conditions T_D. Varying heat intensity $\phi(x_i, x_j)$ and T_D are uniformly sampled to prepare heat source, and the finite element method is employed to solve partial differential equation Eq. (9) for labels. Structured quadrilateral elements are adopted to divide the computational domain, and the solution resolution is 200×200. An example of heat intensity distribution and thermal field is shown in Fig. 3. Finally, a total of 6000 pairs of data are generated. The dataset is split into 4000, 1000, and 1000 samples for training, validation, and testing. The number of sensors is set to 25, uniformly placed on while square domain.

The GCN and GraphSAGE networks are trained for 300 epochs with batch size 8. Adam optimizer with an initial learning rate of 0.001 is adopted. Learning rate is adjusted with exponential decay strategy to ensure that the model is fully trained.

The performance of GCN and GraphSAGE for thermal field reconstruction is shown in Table 1. GCN performs better than GraphSAGE from MAE metrics. The MAE of the two methods is less than 0.3K, which can meet requirements of practical applications. Fig. 4 gives visualization of thermal reconstruction results by GCN. From the contour

DOI: 10.13009/EUCASS2023-612

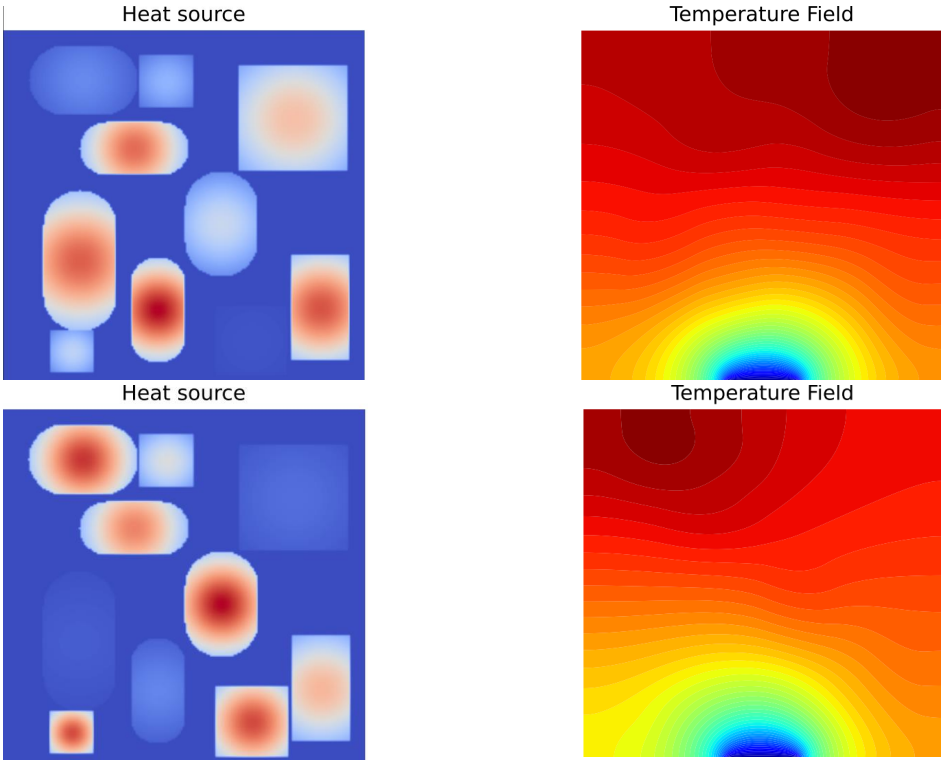

Figure 3: Visualization of heat source map and temperature field map in steady-state thermal field reconstruction case.

line, the reconstructed field has better consistency with the truth. Larger predicted errors are mainly distributed around heat sink, where heat changes greatly.

Table 1: Results of GCN and GraphSAGE networks on thermal field reconstruction with 25 sensors.

Methods	GCN	GraphSAGE
MAE	0.230	0.261

4.2 Compressible Flow over airfoil

This section investigates a flow field reconstruction problem with the proposed GNN-based reconstruction method. To create a complicated scenario close to real-world phenomenons, compressible flow over NACA0012 airfoil with different inlet speeds and attack angles is simulated as the dataset. In this case, a complex turbulent flow occurs around the airfoil. The dataset is prepared by conducting compressible RANS simulation with $k-\omega$ model, in which the attack angles α and Mach number M of free stream condition are selected by uniform sampling. The sampling ranges are set to $[0, 20^{\circ}]$ and $[0.20, 0.85]$, respectively. The sample points are determined with equal intervals to generate a dataset, which contains a total of 2727 snapshots. In the experiments, the dataset is split into 714, 500, and 1513 snapshots for training, validation, and testing.

As shown in Fig. 5, the computational region $[-1, 2] \times [-1, 1]$ is selected for flow field reconstruction, which contains a total of 16339 nodes. Since the grid is refined in local region to ensure the accuracy of numerical simulation, the physical field is not structured data. GNNs are studied due to their flexibility and superior performance for irregular regions, and GCNs and GraphSAGE are implemented as baselines. Besides, POD-based methods are chosen for comparison because it can process complex data. The key issue for POD-based methods is to estimate coefficients of POD modes. In this section, the regression models, including multilayer perceptron, random forest regression, and support vector regression, are implemented as coefficients predictor.

The neural networks are all trained with 300 epochs, and the batch size in each iteration is set to 4. Adam

DOI: 10.13009/EUCASS2023-612

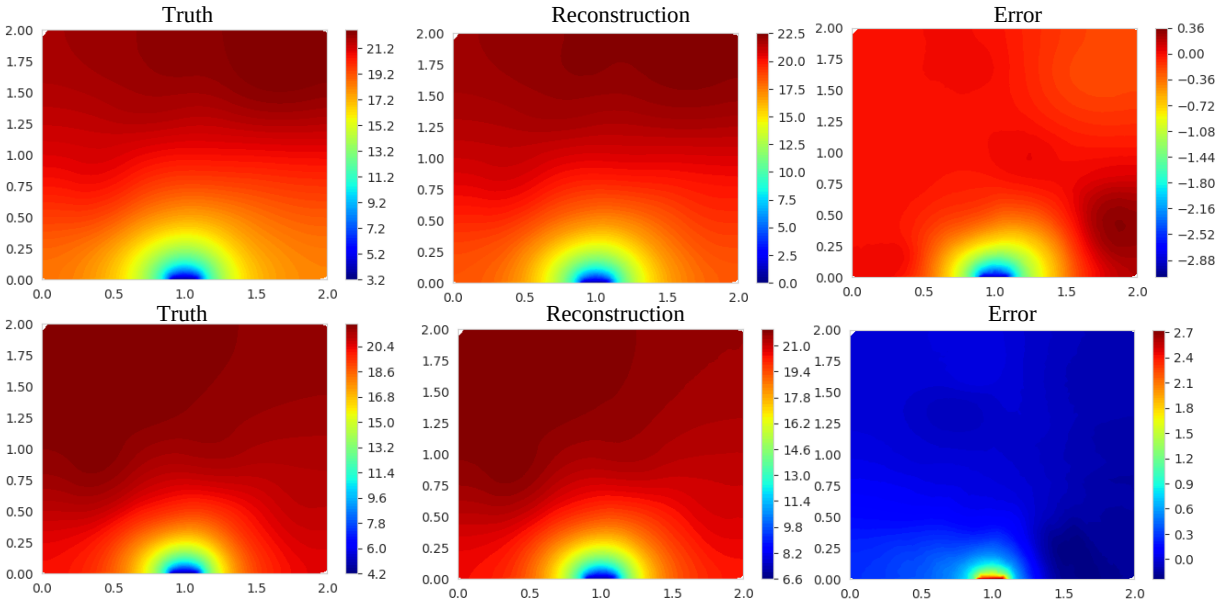

Figure 4: Visualization of thermal field reconstruction by GCN methods.

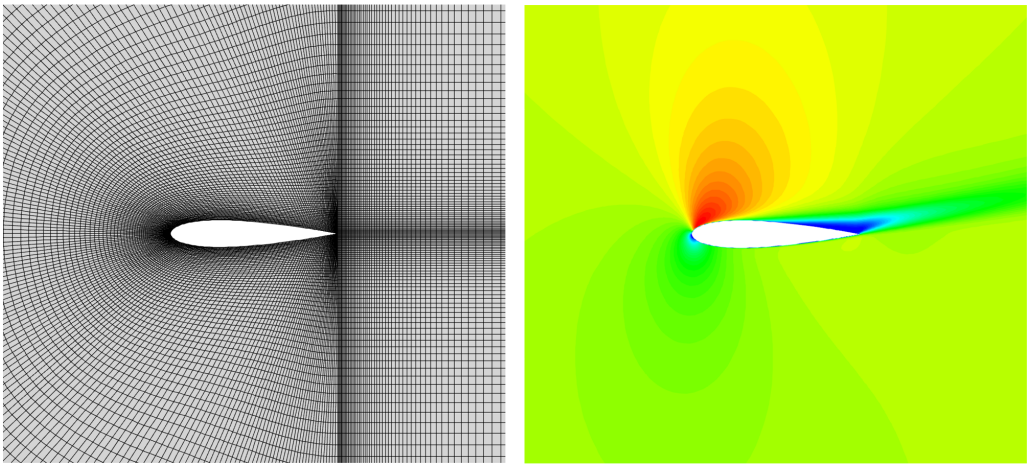

(a) (b)

Figure 5: Illustration of mesh and simulation results over NACA0012 airfoil.

optimizer with an initial learning rate of 0.001 is chosen to optimize network parameters by back propagation algorithm, and learning rate is decayed by a factor of 0.98 in each epoch.

Table 2 gives the results of different reconstruction methods on flow field reconstruction over airfoil. Compared with POD-based methods, GCN and GraphSAGE present competitive results on MAE metrics. GraphSAGE outperforms other methods in most settings, and GCN shows relatively poor performance. The choices of regression models to estimate coefficients are important for POD-based methods. Support vector regression shows a more stable performance for the three regression models and achieves the best pressure reconstruction results. The above results demonstrate that graph neural networks can accurately reconstruct velocity and pressure fields with limited sensors. It is worth noting that the traditional method still performs excellently in this case. The Visualizations of error between labels and reconstructed fields are shown in Fig. 6. Though GNNs show better performance than POD-based methods from MAE metric, the error around airfoil edge is larger. This situation may be caused by the information aggregation in GNNs, which tends to make reconstruction results more smooth.

DOI: 10.13009/EUCASS2023-612

Table 2: Results of different reconstruction methods on compressible flow over NACA0012 airfoil problem. Each approach is evaluated by MAE metrics.

Methods	V_x		V_y		P	
	24	32	24	32	24	32
MLP-POD	1.602	1.640	0.682	0.633	0.217	0.219
RFR-POD	1.944	1.995	0.543	0.535	0.258	0.256
SVR-POD	1.445	1.442	0.603	0.603	0.109	0.111
GCN	4.264	4.289	1.551	1.485	0.271	0.262
GraphSAGE	1.618	1.631	0.521	0.514	0.161	0.176

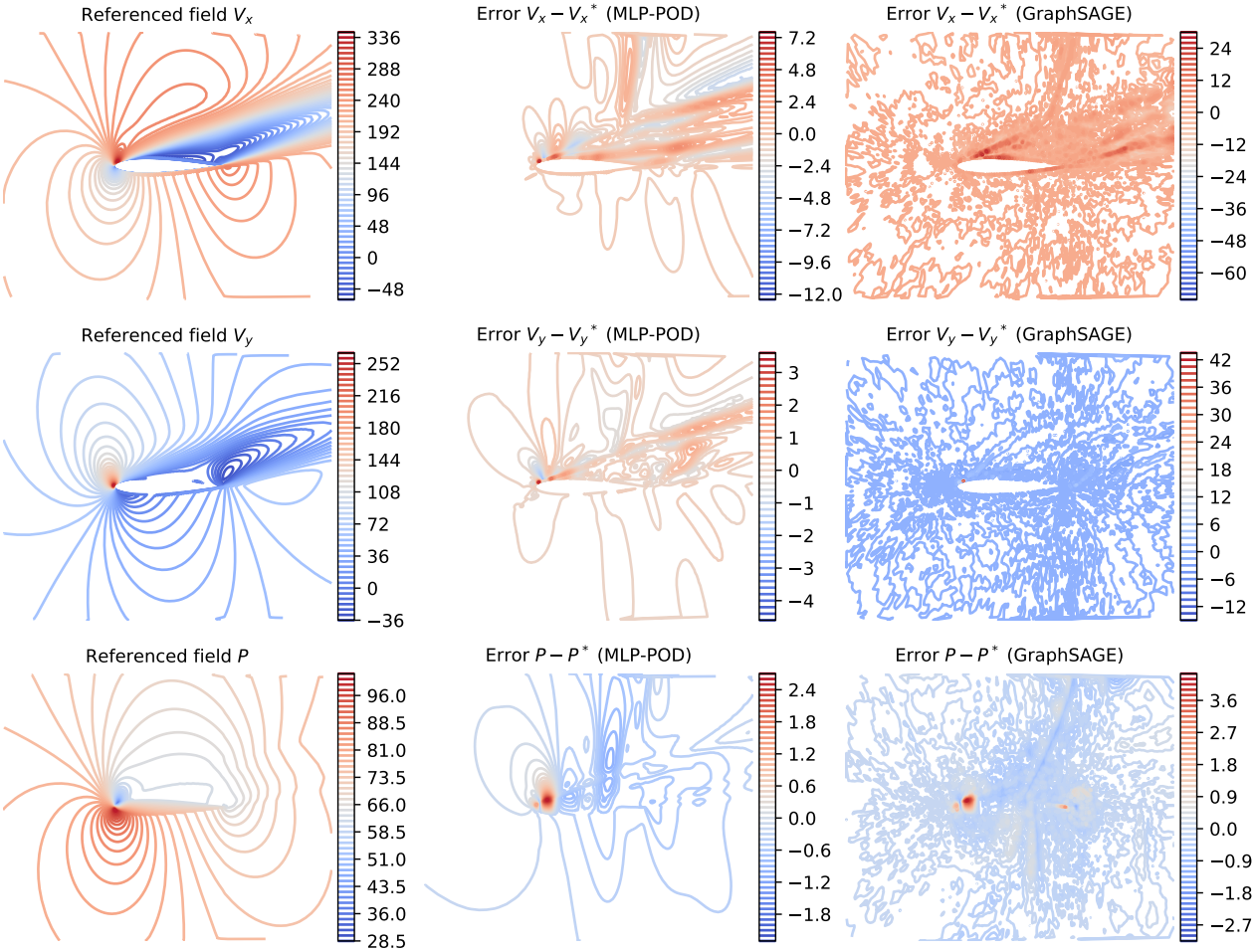

Figure 6: Visualization of results on subsonic and compressible flow over airfoil.

4.3 Temperature Field Reconstruction of On-orbit Satellite

In the last case, monitoring data of one on-orbit satellite is used to investigate the performance of GNN in practical application scenarios. The data includes 2019 and 2020 two-year monitoring data of 120 monitoring points on the satellite, of which 175,200 sets of data are saved every 6 minutes. For 120 measuring points, the temperature data at 40 locations are selected as an input, and the objective is to reconstruct temperature values at the remaining 80 locations. For this case, the model is trained on data of 2019 year and tested on data of the 2020 year.

GCN and GraphSAGE methods are implemented in this section, and FCNN is selected for comparison. All models are trained for a total of 600 epochs, and the batch size is set to 1000. Adam optimizer with 0.01 initial learning rate is adopted to optimize network parameters, and an exponential decay strategy with a multiplicative factor of 0.98 is adopted to adjust learning rate dynamically.

Table 3 shows the results of FCNN, GCN, and GraphSAGE methods in the practical case. From the table,

DOI: 10.13009/EUCASS2023-612

Table 3: Results of different reconstruction methods on actual data.

Methods	MAE	Methods	MAE	Methods	MAE
FCNN	0.25596	GCN	0.23847	GraphSAGE	0.22485

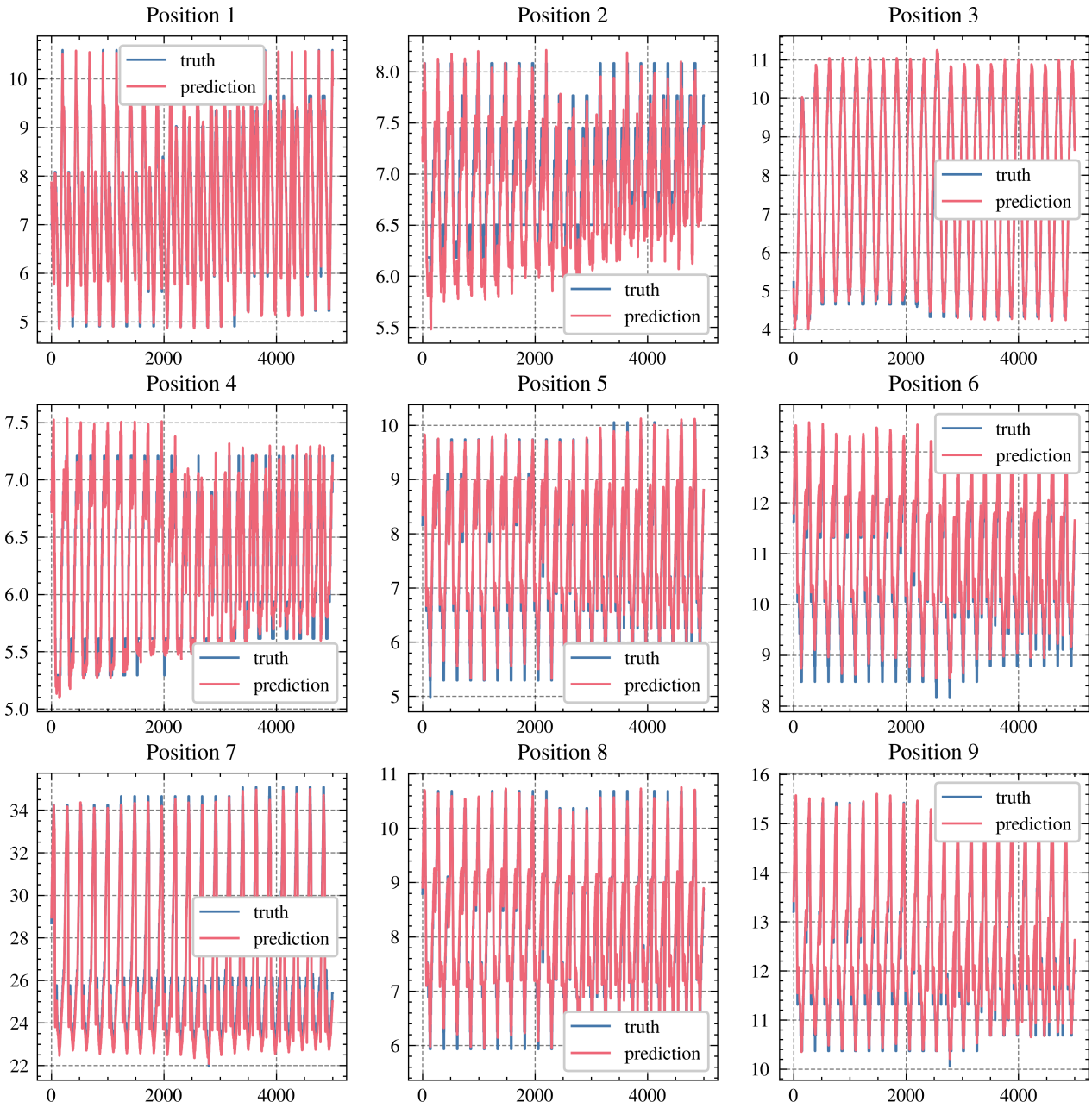

Figure 7: Visualization of reconstruction results on nine positions for on-orbit satellite. The results are provided by GraphSAGE methods

GraphSAGE and GCN outperform FCNN in MAE metric. It is supposed that GraphSAGE and GCN leverage spatial information to obtain more accurate reconstruction results than FCNN. The visualization of reconstruction results of GraphSAGE is presented in Fig. 7. For the nine positions in figure, the trained model can accurately predict temperature leveraging 40 measurements, and the trend of predicted temperature during 5000 times has excellent consistency with exact temperature.

From the results, estimating temperature in more positions with limited measurements in practical scenarios is promising. The biggest challenging is to prepare high-quality training data, which demands that the simulation

DOI: 10.13009/EUCASS2023-612

or practical experiments should be fully carried out in earlier stages. Leveraging the surrogate model with neural network, fewer sensors can be placed on the satellite, and the trained model can provide temperature of more interested positions. Besides, the online data is also valuable in that the model trained with historical data can assist in comparing the predicted results and actual monitoring temperature for abnormal state detection.

5. Conclusion

This paper proposes an end-to-end physical field reconstruction method via graph neural networks from limited sensors. The proposed method adopts a connected graph to represent measurements and the physical field and employs graph neural network to learn the mapping from sensor measurements to global physical field. Graph-based learning can handle irregular domain and unstructured data compared to traditional representations, such as vectors and images. The reconstruction framework based on graph neural network is more flexible and can provide end-to-end reconstruction results accurately. Experiments are conducted on thermal field reconstruction for heat source systems, flow field reconstruction around airfoil, and actual satellite monitoring data. Results demonstrate that graph neural networks can handle field reconstruction of spacecraft from limited sensors and show excellent performance with some settings.

Graph neural networks have some performance bottlenecks that over-smooth situation exits when aggregating neighbor information. For example, the error is larger around airfoil because the physical field has relatively dramatic changes. Besides, graph neural networks are well-known for their difficulty in parameter optimization. In future work, developing a specific architecture for field reconstruction tasks is valuable. Combined with recent studies about physics-informed neural networks, introducing physics laws into model structure design and training is essential to improve method performance and generalization further.

6. Acknowledgment

This work was supported by the National Natural Science Foundation of China (No.52005505).

References

[1] Jared L Callaham, Kazuki Maeda, and Steven L Brunton. Robust flow reconstruction from limited measurements via sparse representation. *Physical Review Fluids*, 4(10):103907, 2019.

[2] Kevin T Carlberg, Antony Jameson, Mykel J Kochenderfer, Jeremy Morton, Liqian Peng, and Freddie D Witherden. Recovering missing cfd data for high-order discretizations using deep neural networks and dynamics learning. *Journal of Computational Physics*, 395:105–124, 2019.

[3] Yumei Ye, Qiang Yang, Fan Yang, Yanyan Huo, and Songhe Meng. Digital twin for the structural health management of reusable spacecraft: a case study. *Engineering Fracture Mechanics*, 234:107076, 2020.

[4] Pin Wu, Junwu Sun, Xuting Chang, Wenjie Zhang, Rossella Arcucci, Yike Guo, and Christopher C Pain. Data-driven reduced order model with temporal convolutional neural network. *Computer Methods in Applied Mechanics and Engineering*, 360:112766, 2020.

[5] David J Lucia, Philip S Beran, and Walter A Silva. Reduced-order modeling: new approaches for computational physics. *Progress in aerospace sciences*, 40(1-2):51–117, 2004.

[6] Kookjin Lee and Kevin T Carlberg. Model reduction of dynamical systems on nonlinear manifolds using deep convolutional autoencoders. *Journal of Computational Physics*, 404:108973, 2020.

[7] Anthony Gruber, Max Gunzburger, Lili Ju, and Zhu Wang. A comparison of neural network architectures for data-driven reduced-order modeling. *Computer Methods in Applied Mechanics and Engineering*, 393:114764, 2022.

[8] Antonios Giannopoulos and Jean-Luc Aider. Data-driven order reduction and velocity field reconstruction using neural networks: The case of a turbulent boundary layer. *Physics of Fluids*, 32(9):095117, 2020.

[9] Zhiwen Deng, Yujia Chen, Yingzheng Liu, and Kyung Chun Kim. Time-resolved turbulent velocity field reconstruction using a long short-term memory (lstm)-based artificial intelligence framework. *Physics of Fluids*, 31(7):075108, 2019.

DOI: 10.13009/EUCASS2023-612

[10] Joshua L Proctor, Steven L Brunton, and J Nathan Kutz. Dynamic mode decomposition with control. *SIAM Journal on Applied Dynamical Systems*, 15(1):142–161, 2016.

[11] Clarence W Rowley and Scott TM Dawson. Model reduction for flow analysis and control. *Annu. Rev. Fluid Mech*, 49(1):387–417, 2017.

[12] Richard Everson and Lawrence Sirovich. Karhunen–loeve procedure for gappy data. *JOSA A*, 12(8):1657–1664, 1995.

[13] Bérengre Podvin, Yann Fraigneau, François Lusseyran, and Pierre Gougat. A reconstruction method for the flow past an open cavity. 2006.

[14] Lionel Mathelin, Kévin Kasper, and Hisham Abou-Kandil. Observable dictionary learning for high-dimensional statistical inference. *Archives of Computational Methods in Engineering*, 25(1):103–120, 2018.

[15] Jiayang Xu and Karthik Duraisamy. Multi-level convolutional autoencoder networks for parametric prediction of spatio-temporal dynamics. *Computer Methods in Applied Mechanics and Engineering*, 372:113379, 2020.

[16] Yasi Wang, Hongxun Yao, and Sicheng Zhao. Auto-encoder based dimensionality reduction. *Neurocomputing*, 184:232–242, 2016.

[17] Yash Kumar, Pranav Bahl, and Souvik Chakraborty. State estimation with limited sensors–a deep learning based approach. *Journal of Computational Physics*, 457:111081, 2022.

[18] Antonia Creswell, Tom White, Vincent Dumoulin, Kai Arulkumaran, Biswa Sengupta, and Anil A Bharath. Generative adversarial networks: An overview. *IEEE signal processing magazine*, 35(1):53–65, 2018.

[19] Jeremy Morton, Mykel J Kochenderfer, and Freddie D Witherden. Parameter-conditioned sequential generative modeling of fluid flows. *AIAA Journal*, 59(3):825–841, 2021.

[20] Nirmal J Nair and Andres Goza. Leveraging reduced-order models for state estimation using deep learning. *Journal of Fluid Mechanics*, 897, 2020.

[21] Pierre Dubois, Thomas Gomez, Laurent Planckaert, and Laurent Perret. Machine learning for fluid flow reconstruction from limited measurements. *Journal of Computational Physics*, 448:110733, 2022.

[22] N Benjamin Erichson, Lionel Mathelin, Zhewei Yao, Steven L Brunton, Michael W Mahoney, and J Nathan Kutz. Shallow neural networks for fluid flow reconstruction with limited sensors. *Proceedings of the Royal Society A*, 476(2238):20200097, 2020.

[23] Jonathan Long, Evan Shelhamer, and Trevor Darrell. Fully convolutional networks for semantic segmentation. In *Proceedings of the IEEE conference on computer vision and pattern recognition*, pages 3431–3440, 2015.

[24] Zhiqiang Gong, Ping Zhong, Yang Yu, Weidong Hu, and Shutao Li. A cnn with multiscale convolution and diversified metric for hyperspectral image classification. *IEEE Transactions on Geoscience and Remote Sensing*, 57(6):3599–3618, 2019.

[25] Tianyuan Liu, Yunzhu Li, Qi Jing, Yonghui Xie, and Di Zhang. Supervised learning method for the physical field reconstruction in a nanofluid heat transfer problem. *International Journal of Heat and Mass Transfer*, 165:120684, 2021.

[26] Zhiqiang Gong, Weien Zhou, Jun Zhang, Wei Peng, and Wen Yao. Physics-informed deep reversible regression model for temperature field reconstruction of heat-source systems. *arXiv preprint arXiv:2106.11929*, 2021.

[27] Xingwen Peng, Xingchen Li, Zhiqiang Gong, Xiaoyu Zhao, and Wen Yao. A deep learning method based on partition modeling for reconstructing temperature field. *International Journal of Thermal Sciences*, 182:107802, 2022.

[28] Kai Fukami, Romit Maulik, Nesar Ramachandra, Koji Fukagata, and Kunihiko Taira. Global field reconstruction from sparse sensors with voronoi tessellation-assisted deep learning. *Nature Machine Intelligence*, 3(11):945–951, 2021.

[29] Jiaqi Han, Wenbing Huang, Hengbo Ma, Jiachen Li, Josh Tenenbaum, and Chuang Gan. Learning physical dynamics with subequivariant graph neural networks. *Advances in Neural Information Processing Systems*, 35:26256–26268, 2022.

DOI: 10.13009/EUCASS2023-612

[30] Junfeng Chen, Elie Hachem, and Jonathan Viquerat. Graph neural networks for laminar flow prediction around random two-dimensional shapes. *Physics of Fluids*, 33(12):123607, 2021.

[31] Joosep Pata, Javier Duarte, Jean-Roch Vlimant, Maurizio Pierini, and Maria Spiropulu. Mlpf: efficient machine-learned particle-flow reconstruction using graph neural networks. *The European Physical Journal C*, 81:1–14, 2021.

[32] Florent Bonnet, Jocelyn Ahmed Mazari, Paola Cinella, and Patrick Gallinari. Airfrans: High fidelity computational fluid dynamics dataset for approximating reynolds-averaged navier-stokes solutions. In *36th Conference on Neural Information Processing Systems (NeurIPS 2022) Track on Datasets and Benchmarks*, 2022.

[33] Xiaoyu Zhao, Zhiqiang Gong, Jun Zhang, Wen Yao, and Xiaoqian Chen. A surrogate model with data augmentation and deep transfer learning for temperature field prediction of heat source layout. *Structural and Multidisciplinary Optimization*, 64(4):2287–2306, 2021.

[34] Zhiqiang Gong, Weien Zhou, Jun Zhang, Wei Peng, and Wen Yao. Joint deep reversible regression model and physics-informed unsupervised learning for temperature field reconstruction. *Engineering Applications of Artificial Intelligence*, 118:105686, 2023.

[35] Xiaoyu Zhao, Zhiqiang Gong, Yunyang Zhang, Wen Yao, and Xiaoqian Chen. Physics-informed convolutional neural networks for temperature field prediction of heat source layout without labeled data. *Engineering Applications of Artificial Intelligence*, 117:105516, 2023.